

Atomic-Scale Study of Plastic-Yield Criterion in Nanocrystalline Cu at High Strain Rates

A.M. DONGARE, A.M. RAJENDRAN, B. LAMATTINA, D.W. BRENNER,
and M.A. ZIKRY

Large-scale molecular dynamics (MD) simulations are used to understand the macroscopic yield behavior of nanocrystalline Cu with an average grain size of 6 nm at high strain rates. The MD simulations at strain rates varying from 10^9 s^{-1} to $8 \times 10^9 \text{ s}^{-1}$ suggest an asymmetry in the flow stress values in tension and compression, with the nanocrystalline metal being stronger in compression than in tension. The tension-compression strength asymmetry is very small at 10^9 s^{-1} , but increases with increasing strain rate. The calculated yield stresses and flow stresses under combined biaxial loading conditions (X - Y) gives a locus of points that can be described with a traditional ellipse. An asymmetry parameter is introduced that allows for the incorporation of the small tension-compression asymmetry. The biaxial yield surface (X - Y) is calculated for different values of stress in the Z direction, the superposition of which gives a full three-dimensional (3-D) yield surface. The 3-D yield surface shows a cylinder that is symmetric around the hydrostatic axis. These results suggest that a von Mises-type yield criterion can be used to understand the macroscopic deformation behavior of nanocrystalline Cu with a grain size in the inverse Hall-Petch regime at high strain rates.

DOI: 10.1007/s11661-009-0113-x

© The Minerals, Metals & Materials Society and ASM International 2009

I. INTRODUCTION

NANOCRYSTALLINE metals, due to their enhanced strength and wear resistance, show significant promise for a number of future high-technology applications such as microelectromechanical systems, nanoelectromechanical systems, and nanoscale devices. To maximize the performance and reliability of these devices, a fine-tuning of the nanostructure is required, which necessitates a fundamental understanding of the deformation and failure mechanisms.^[1] Nanocrystalline metals have been extensively studied,^[2-9] to understand the micromechanisms governing their macroscopic mechanical behavior. At the atomic scale, plastic deformation mechanisms in nanocrystalline materials can be classified into dislocation-based and grain-boundary (GB)-based processes. A reduction in grain size results in an increase in the yield strength of materials, a relation known as the Hall-Petch effect,^[10] which states that the yield strength varies inversely with the square root of the grain size. Recent studies^[11-14] indicate that the increase in strength with decreasing grain size

reaches a maximum after which a further decrease in the grain size (less than $\sim 12 \text{ nm}$) can result in weakening of the metal. This weakening of the metal, due to the shift in the dominating mechanism of plastic deformation from dislocation-induced plasticity in the case of coarse-grained materials to GB sliding in the case of ultrasmall grain sizes, is referred to as the inverse Hall-Petch behavior.^[15]

Nanocrystalline metals with ultrasmall grain sizes ($d \leq 30 \text{ nm}$) have gained considerable attention due to their increased strengths during deformation at high strain rates.^[16] In addition, shock loading of these ultrasmall nanocrystalline metals at speeds that are greater than the speed of sound (strain rates $\geq 10^8 \text{ s}^{-1}$) limits the GB sliding mechanism and thus results in ultrahigh strength values for the nanocrystalline metal.^[17] This limiting of GB sliding at ultrahigh strain rates may lead to modifications in the yield criteria/behavior at the ultrasmall grain sizes. To maximize the performance and reliability of these devices, a fine-tuning of the nanostructure is required, which necessitates a fundamental understanding of the deformation and failure of the constituent materials of the devices.

The macroscopic response of materials to plastic deformation can be understood by calculating the yield criterion governing the multiaxial plasticity at high strain rates. The most commonly used phenomenological yield criteria^[18,19] for polycrystalline metals, such as von Mises and Tresca, are based on the assumption that the yielding of the metal is determined by the deviatoric stress and is independent of the pressure and the normal stress. These conventional yield criteria have been found to be appropriate to study deformation behavior in polycrystalline metals.^[18,19] Plasticity in polycrystalline

A.M. DONGARE, NRC Research Associate, Department of Mechanical and Aerospace Engineering and Department of Materials Science and Engineering, D.W. BRENNER, Kobe Steel Distinguished Professor, Department of Materials Science and Engineering, and M.A. ZIKRY, Professor, Department of Mechanical and Aerospace Engineering, are with North Carolina State University, Raleigh, NC 27695-7907. Contact e-mail: amdongare@ncsu.edu A.M. RAJENDRAN, Chair and Professor, is with the Department of Mechanical Engineering, University of Mississippi, Oxford, MS 38677. B. LAMATTINA, Program Manager, is with the United States Army Research Office, Research Triangle Park, NC 27703.

Manuscript submitted April 1, 2009.

Article published online December 2, 2009

Report Documentation Page				Form Approved OMB No. 0704-0188	
Public reporting burden for the collection of information is estimated to average 1 hour per response, including the time for reviewing instructions, searching existing data sources, gathering and maintaining the data needed, and completing and reviewing the collection of information. Send comments regarding this burden estimate or any other aspect of this collection of information, including suggestions for reducing this burden, to Washington Headquarters Services, Directorate for Information Operations and Reports, 1215 Jefferson Davis Highway, Suite 1204, Arlington VA 22202-4302. Respondents should be aware that notwithstanding any other provision of law, no person shall be subject to a penalty for failing to comply with a collection of information if it does not display a currently valid OMB control number.					
1. REPORT DATE 2010		2. REPORT TYPE		3. DATES COVERED 00-00-2010 to 00-00-2010	
4. TITLE AND SUBTITLE Atomic-Scale Study of Plastic-Yield Criterion in Nanocrystalline Cu at High Strain Rates				5a. CONTRACT NUMBER	
				5b. GRANT NUMBER	
				5c. PROGRAM ELEMENT NUMBER	
6. AUTHOR(S)				5d. PROJECT NUMBER	
				5e. TASK NUMBER	
				5f. WORK UNIT NUMBER	
7. PERFORMING ORGANIZATION NAME(S) AND ADDRESS(ES) Department of Mechanical and Aerospace Engineering and,Department of Materials Science and Engineering ,North Carolina State University,Raleigh,NC,27695-7907				8. PERFORMING ORGANIZATION REPORT NUMBER	
9. SPONSORING/MONITORING AGENCY NAME(S) AND ADDRESS(ES)				10. SPONSOR/MONITOR'S ACRONYM(S)	
				11. SPONSOR/MONITOR'S REPORT NUMBER(S)	
12. DISTRIBUTION/AVAILABILITY STATEMENT Approved for public release; distribution unlimited					
13. SUPPLEMENTARY NOTES					
14. ABSTRACT					
15. SUBJECT TERMS					
16. SECURITY CLASSIFICATION OF:			17. LIMITATION OF ABSTRACT Same as Report (SAR)	18. NUMBER OF PAGES 10	19a. NAME OF RESPONSIBLE PERSON
a. REPORT unclassified	b. ABSTRACT unclassified	c. THIS PAGE unclassified			

metals is dominated by the nucleation and propagation of dislocations. Plasticity in nanocrystalline metals, however, has contributions from dislocation-based and GB-based processes. The GB processes become more dominant at grain sizes less than 30 nm. Particularly important is the case of nanocrystalline metals with the grain size in the inverse Hall–Petch regime ($d \leq 15$ nm) in which GB sliding dominates the deformation behavior.^[20] Deformation studies of nanocrystalline metals (2 to 4 nm) using molecular static simulations indicate a strong asymmetry in tensile and compressive strengths.^[21] A similar behavior is observed in metallic glasses, in which a strong asymmetry in tension and compression is observed and can be well described using the Mohr–Coulomb criterion, which accounts for a normal stress dependence.^[22,23] This normal stress-dependent criterion has been recently extended to the ultrasmall grains (2 nm), suggesting that ultrasmall grains can be considered as amorphous materials at the lower limit of the grain size.^[24]

To date, most of the crystal plasticity models developed to describe plastic deformation and failure in conventional coarse-grained metals do not explicitly include GB effects on plasticity. As a result, these models may not be suitable for predicting the material response at grain sizes in the inverse Hall–Petch regime. The modification of conventional continuum failure models to accurately predict material behavior at the nanoscale would represent a paradigm shift in the design and realization of revolutionary nanocrystalline materials. The molecular dynamics (MD) simulation technique has the potential to provide the atomic-level structural information about the deformation mechanisms needed to modify and expand the capabilities of continuum simulations. The focus of this article is to understand the response of these ultrasmall-grain-size nanocrystalline metals during deformation under conditions of multi-axial loading. The strain rates used here are chosen to reproduce those observed during shock loading to create ultrahigh strengths in nanocrystalline metals.^[17] Shock loading using short (nanosecond) laser pulses leads to peak strain rates exceeding 10^7 s^{-1} ,^[25–27] whereas the use of ultrashort (femtosecond) laser pulses results in strain rates exceeding 10^8 s^{-1} .^[28,29] As a result, MD simulations are carried out to understand the macroscopic deformation behavior of nanocrystalline Cu with an average grain size of 6 nm at ultrahigh strain rates ($\geq 10^8 \text{ s}^{-1}$). Three aspects of deformation behavior are studied: the tension-compression strength asymmetry, the biaxial yield surface, and the three-dimensional (3-D) yield surface. The computational details are presented in Section II. The tension-compression strength asymmetry is discussed in Section III, followed by the calculation of the 3-D yield surface in Section IV.

II. COMPUTATIONAL METHODS

The initial MD system of nanocrystalline Cu used in this study is created by the Voronoi construction method, as suggested by Derlet and Van Swygenhoven.^[30] Periodic boundary conditions are used in all

three directions. In addition, the system is equilibrated at 300 K for 200 picoseconds to relax the structure after the Voronoi construction. The density of the final configuration is calculated to be ~99 pct of the bulk density of copper. This procedure constructs a system with random grain orientations containing no textures and a grain size distribution close to a log-normal distribution.^[31] The centrosymmetry parameter (Δ_{CSP})^[32] is calculated for each atom as

$$\Delta_{\text{CSP}} = \sum_{i=1,6} |R_i + R_{i+6}|^2 \quad [1]$$

The blue color ($\Delta_{\text{CSP}} \sim 0$) corresponds to FCC stacking; the green color ($\Delta_{\text{CSP}} \sim 8$) represents grain boundaries and partial dislocations; and the red color ($\Delta_{\text{CSP}} > 15$) represents a surface. A typical system with an average grain size of 6 nm and containing 122 grains is shown in Figure 1, with the atoms colored according to the Δ_{CSP} values. The system consists of approximately 1.2 million atoms arranged in 122 grains with an average grain diameter of ~6 nm. The MD simulations are carried out using the Voter–Chen (VC) formulation^[33] of the embedded atom method potential for copper. The VC potential provides a good description of the unstable and stable stacking fault energies and therefore is well suited to describe deformation behavior for Cu.^[34]

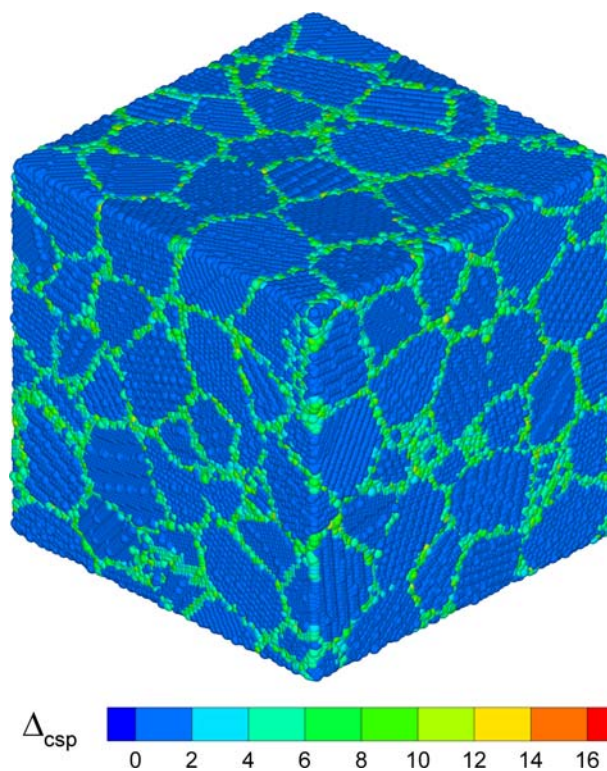


Fig. 1—Initial configuration of nanocrystalline Cu with an average grain size of 6 nm. System consists of approximately 1.2 million atoms arranged in 122 grains; each atom is colored according to the Δ_{CSP} .

The elements of the tensor of atomic-level stresses are calculated as

$$\sigma_{\alpha\beta}(i) = -\frac{1}{\Omega_0} \left[\frac{1}{2} \sum_j F_{ij}^\alpha r_{ij}^\beta + M_i v_i^\alpha v_i^\beta \right] \quad [2]$$

where α and β are the Cartesian components, Ω_0 is the atomic volume, F_{ij} is the force on atom i due to atom j , M_i is the mass of atom i , and v_i is the velocity of atom i . An effective stress (σ_e) and an effective strain (ϵ_e) according to the von Mises criterion for yielding is calculated as

$$\sigma_e = \left[\frac{1}{2} \left((\sigma_x - \sigma_y)^2 + (\sigma_y - \sigma_z)^2 + (\sigma_z - \sigma_x)^2 + 6(\sigma_{xy}^2 + \sigma_{yz}^2 + \sigma_{xz}^2) \right) \right]^{1/2} \quad [3]$$

$$\epsilon_e = \frac{\sqrt{2}}{3} \left[\left((\epsilon_x - \epsilon_y)^2 + (\epsilon_y - \epsilon_z)^2 + (\epsilon_z - \epsilon_x)^2 \right) \right]^{1/2} \quad [4]$$

where σ_x , σ_y , and σ_z are the stresses averaged over the entire system in the X , Y , and Z directions, respectively, and ϵ_x , ϵ_y , and ϵ_z are the engineering strains in the X , Y , and Z directions, respectively. The time-step for all of the MD simulation runs is chosen to be 0.002 ps. The temperature is allowed to evolve during the deformation process. The effect of ultrahigh strain rate deformation on the strength asymmetry is discussed in Section III along with the predicted plastic-yield surface.

III. TENSION-COMPRESSION STRENGTH ASYMMETRY IN NANOCRYSTALLINE Cu

The MD simulations of uniaxial loading of the nanocrystalline Cu sample are carried out at constant strain by deforming the sample in the X direction, and maintaining zero stress conditions in the Y and Z directions ($\sigma_y = \sigma_z = 0$ and $\sigma_x = \sigma$). At each time-step, deformation is achieved by adjusting the x coordinate of all the atoms and, accordingly, the length of the system, in the X direction by a scaling parameter chosen to achieve the desired strain rate ($\dot{\epsilon}$). The coordinates in the Y and Z directions are scaled so as to have zero stress in the Y and Z directions. The MD simulations of deformation are carried out for strain rates ranging from $1 \times 10^9 \text{ s}^{-1}$ to $8 \times 10^9 \text{ s}^{-1}$. The choice of strain rates is based on those generated during shock loading using picosecond and femtosecond laser pulses.^[17,28,29] Based on Eqs. [3] and [4], for the conditions of uniaxial stress loading, the effective von Mises stress (σ_e) reduces to the stress in the loading direction (σ_x), and the effective strain (ϵ_e) reduces to the strain in the loading direction (ϵ_x). The plots of the effective von Mises stress as a function of effective strain during uniaxial deformation in tension in comparison with that in compression are shown for strain rates of $1 \times 10^9 \text{ s}^{-1}$ to $8 \times 10^9 \text{ s}^{-1}$ in Figure 2. The curves are initially linear up to the yield point, after which they start

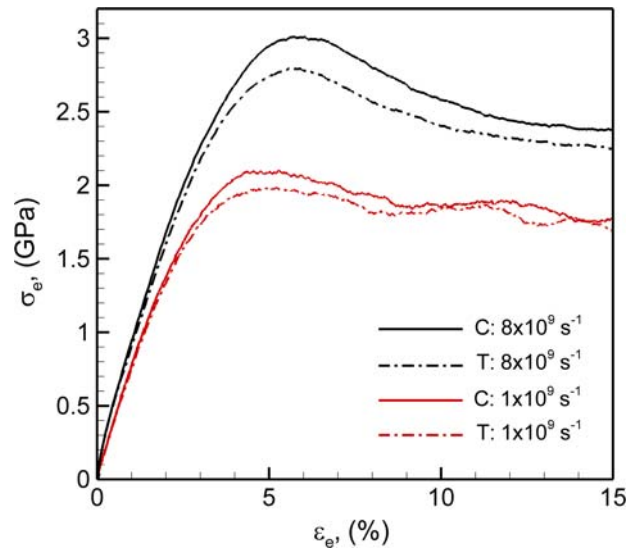


Fig. 2—Plots of effective von Mises stress as a function of effective strain in tension and compression at strain rates of $1 \times 10^9 \text{ s}^{-1}$ and $8 \times 10^9 \text{ s}^{-1}$, respectively. Nanocrystalline Cu shows greater strength in compression (C) as compared to tension (T).

Table I. Values of Flow (Peak) Stress during Uniaxial Deformation of Nanocrystalline Cu with an Average Grain Size of 6 Nanometers at Various Strain Rates in Tension and Compression

Strain Rate $\dot{\epsilon}$ (s^{-1})	Tension (Flow Stress) σ_f^T (GPa)	Compression (Flow Stress) σ_f^C (GPa)	Strength Asymmetry (Pct)
1×10^9	1.986	2.101	5.79
2×10^9	2.164	2.303	6.42
4×10^9	2.405	2.577	7.15
8×10^9	2.794	3.010	7.73
1×10^{11}	6.399	8.712	36.15

to deviate from elastic behavior. The flow stress (σ_f) is defined as the peak stress in the stress-strain curve.^[12,24] The nanocrystalline Cu is observed to be stronger in compression than in tension. This strength asymmetry, defined as the tension-compression strength differential,^[21,24] is larger at the higher strain rates. The calculated values of the flow stress in tension and compression at various strain rates are tabulated in Table I and plotted in Figure 3. The nanocrystalline sample shows a strength asymmetry of ~8 pct at $8 \times 10^9 \text{ s}^{-1}$, which is much lower than that (~35 pct) observed in nanocrystalline Ni during quasi-static loading using molecular static simulations.^[27] It should be noted that the quasi-static deformation is obtained by scaling the atomic coordinates (strain increments along the axis) followed by relaxation of the system using the conjugant gradient technique.^[21,24] This relaxation in molecular static simulations, however, does not allow for complete adiabatic relaxation of the system during the deformation process. The deformation strains

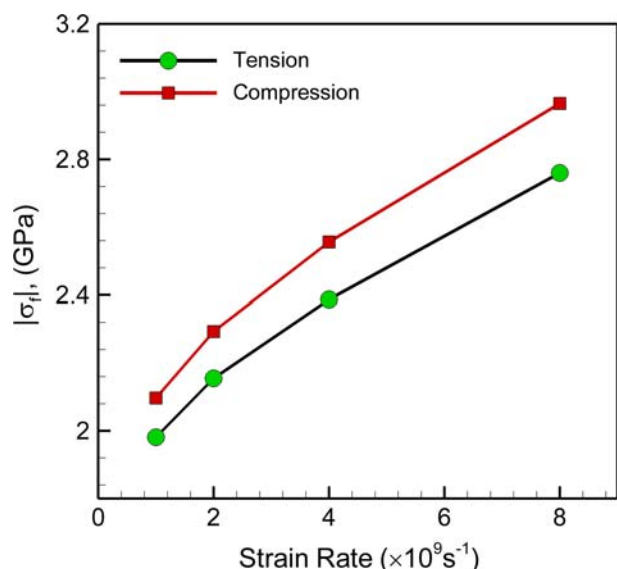


Fig. 3—Plot of the calculated yield stress and flow (peak) stress in tension and compression at strain rates $1 \times 10^9 \text{ s}^{-1}$ to $8 \times 10^9 \text{ s}^{-1}$, respectively. Yield stress and flow stress values are greater in compression and the difference increases with increasing strain rates.

used may therefore result in deformation at ultrahigh strain rates, which results in the large strength asymmetry (~35 pct) in tension and compression for nanocrystalline Ni. To test this, the flow stress is calculated for uniaxial stress loading in tension and compression using MD simulations at a strain rate of 10^{11} s^{-1} . The tension-compression strength asymmetry is calculated to be ~36 pct at a strain rate of 10^{11} s^{-1} . This value of the asymmetry compares very well with that observed for quasi-static loading of nanocrystalline Ni and suggests that the large asymmetry observed in quasi-static deformation of Ni using molecular static simulations may be due to the unusually high strain rates of deformation induced by the technique.

IV. PLASTIC-YIELD SURFACE

A full 3-D plastic yield surface using MD simulations can be obtained by deforming the nanocrystalline metal by equal/unequal amounts in the X , Y , and Z directions and plotting the plastic yield/flow stresses in the X , Y , and Z axes. While the process can be complicated and in turn tedious, the 3-D yield surface can also be obtained by computing the biaxial yield surfaces. Here, in this work, the biaxial yield surface is calculated by plotting the yield/flow stresses during loading of the nanocrystalline metal by equal/unequal amounts in the X and Y directions and keeping the stress in the Z direction constant ($\sigma_z = 0 \text{ GPa}$). The biaxial yield surface is then calculated in a similar way for different values of the constant stress in the Z direction ($\sigma_z = 1 \text{ GPa}$; $\sigma_z = -1 \text{ GPa}$). The calculated biaxial yield surfaces are then superimposed along the Z axis to obtain a 3-D yield surface.

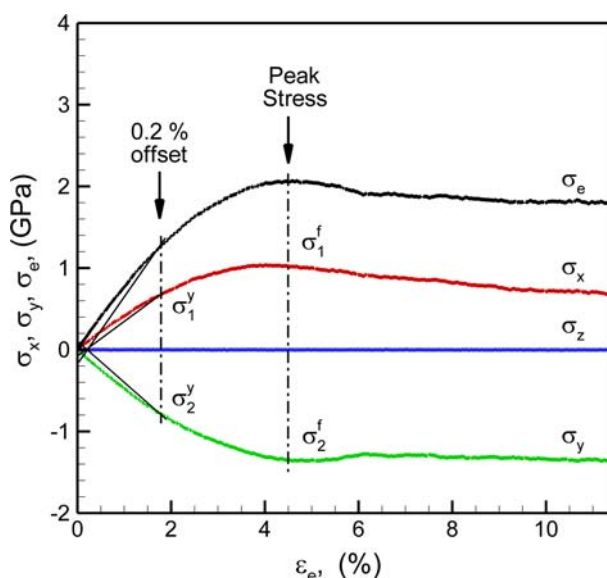


Fig. 4—Evolution of the stresses in the X , Y , and Z directions, along with the effective von Mises stress as a function of effective strain for unbalanced biaxial loading (X in tension and Y in compression shown). Yield stresses in X and Y directions are calculated based on the 0.2 pct offset stress on the von Mises curve. Flow stress in the X and Y directions is calculated at the value of the effective strain corresponding to a peak in the von Mises curve. Effective strains corresponding to the yield stress and flow stress are shown by the dashed-dotted lines.

A. Biaxial Yield Surface at $\sigma_z = 0 \text{ GPa}$

The initial nanocrystalline Cu system is equilibrated at zero pressure for 50 ps to have a stress of $\sigma_z = 0 \text{ GPa}$ in the X , Y , and Z directions. To calculate the biaxial yield surface, deformation is achieved at each time-step by adjusting the x and y coordinates of all the atoms by a scaling parameter based on the loading conditions in the X and Y directions. The scaling in the X and Y directions may be equal or unequal depending on the desired combination of stresses desired ($\sigma_x = \sigma_1$, $\sigma_y = \sigma_2$, and $\sigma_z = \sigma_3 = 0$). The maximum scaling used gives a strain rate of 10^9 s^{-1} . For the case of unbalanced deformation in the X and Y directions, the calculation of yield stresses and flow stresses can be complicated. For example, Figure 4 shows the evolution of the stresses averaged in the X , Y , and Z directions, along with the von Mises stress as a function of effective strain. The deformation conditions correspond to tensile loading in the X direction and compressive loading in Y direction. Yielding is defined by the 0.2 pct offset stress in each direction, as shown by the black lines in Figure 4. It can be seen that the yielding on the effective stress curve occurs at the same value of effective strain as observed for yielding in the X and Y directions. As a result, for the various combinations of loading conditions, the yield stress values in the X direction (σ_1^y) and Y direction (σ_2^y) are calculated at the effective strain corresponding to the 0.2 pct offset stress on the effective stress curve (σ_e^y). Similarly, the flow stress (peak value of the stress) values in the X direction (σ_1^f) and Y direction (σ_2^f) are calculated at the effective strain corresponding to the

peak value of the effective stress curve (σ'_e). The effective strains corresponding to the yield stress and flow stress are shown by the dashed-dotted lines in Figure 4.

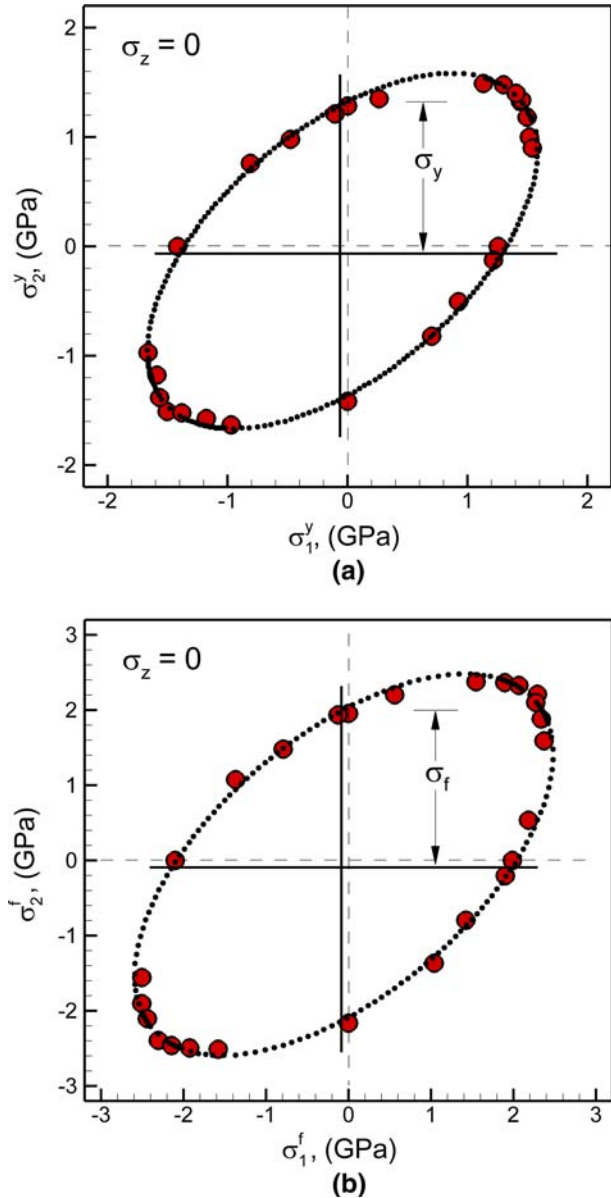


Fig. 5—Plot of the locus of (a) the yield stress (0.2 pct offset stress) values and (b) flow stress (peak value of stress) values, for biaxial loading in the X and Y directions and zero stress in the Z direction. Dotted ellipse fitted to the data suggests a von Mises-type yield surface. Solid lines indicate the shifted center of the ellipse to account for the tension-compression strength asymmetry.

The locus of the yield stress values and flow stress values for biaxial loading ($\sigma_x = \sigma_1$, $\sigma_y = \sigma_2$, and $\sigma_3 = \sigma_z = 0$) is shown in Figures 5(a) and (b), respectively. The yield and flow surfaces can be fitted to an ellipse (dotted), as shown, and suggests a von Mises-type surface for yielding. The center of the ellipse, however, is shifted by a very small amount in the third quadrant in order to fit the yield surface. This shift in the center of the ellipse is due to the inherent tension-compression strength asymmetry at these high strain rates. The amount of shift in the center of the ellipse is defined as an asymmetry parameter (α) and is symmetric in the X and Y directions. The traditional von Mises ellipse has the minor and major axis lengths defined as $(\sqrt{2/3})\sigma_y$ and $(\sqrt{2})\sigma_y$, respectively, where σ_y is the calculated yield stress in tension. The yield stress and flow stress values for the fitted ellipse are calculated from the shifted center of the ellipse, as shown in Figures 5(a) and (b), respectively. The parameters of the fitted ellipse for the yield stresses give the length of the minor axis to be 1.05 GPa, which compares very well with the value of ~ 1.06 GPa predicted by a traditional von Mises ellipse using σ_y . The length for the major axis for the fitted ellipse is calculated to be 2.03 GPa, which is slightly larger than the value of ~ 1.84 GPa predicted by a traditional von Mises ellipse using σ_y . Similarly, the flow stress ellipse has a minor axis of 1.64 GPa, which agrees very well with the value of ~ 1.67 GPa predicted by a traditional von Mises ellipse using σ_f . The length of the major axis for the flow stress ellipse is calculated to be 3.19 GPa, which is slightly larger than the value of ~ 2.9 GPa predicted by a traditional von Mises ellipse using σ_f . Thus, the ellipse fitted to the yield locus suggests the validity of the von Mises-type yield criterion, but deviates slightly in the length of the major axis or, in other words, the aspect ratio of the predicted ellipse. A similar fitting can be done for the Tresca criterion. The calculated lengths of the major and minor axis are tabulated in Table II, along with the asymmetry parameter.

B. Biaxial Yield Surface at $\sigma_z = 1$ GPa

To calculate the yield stresses at a stress of 1 GPa in the Z direction, the system is first equilibrated for 100 ps at a pressure of $P = -1$ GPa. As a result, the stresses in the X , Y , and Z directions are equilibrated at 1 GPa prior to deformation. The deformation is then carried out by scaling the x and y coordinates of the atoms by equal or unequal amounts, depending on the desired combination of loading conditions in the X and Y

Table II. Calculated Lengths of Major and Minor Axes of Ellipse Used to Fit Biaxial Yield and Flow Surfaces at Various Constant Values of Stress; σ_y and σ_z are Yield Stress and Flow Stress Values, Respectively, in Tension with Shifted Center of Ellipse; α_y and α_f are the Shift in the Center of the Ellipse from the Ideal Value

Z Stress (GPa)	Yield Stress				Flow Stress			
	Minor Axis	Major Axis	σ_y	α_y	Minor Axis	Major Axis	σ_f	α_f
$\sigma_z = 0$	1.05	2.03	1.30	0.04	1.64	3.19	2.05	0.06
$\sigma_z = +1$	1.075	2.15	1.38	0.12	1.60	3.10	2.00	0.05
$\sigma_z = -1$	1.2	2.25	1.50	0.10	1.66	3.35	2.09	0.06

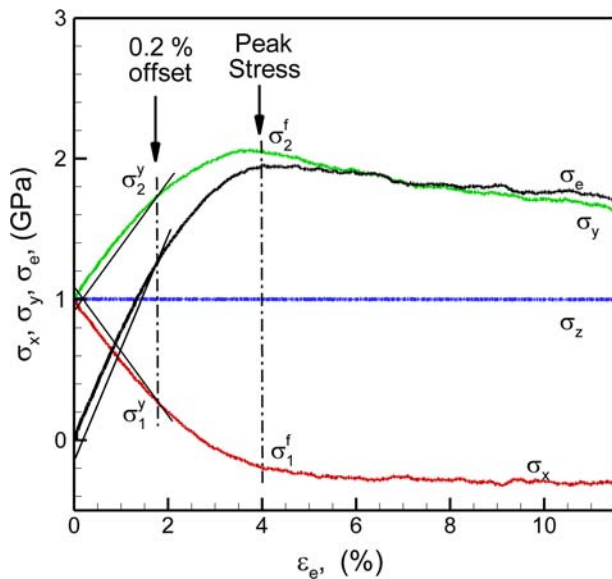


Fig. 6—Evolution of the stresses in the X , Y , and Z directions, along with the effective von Mises stress as a function of the effective strain for unbalanced biaxial loading (X in compression and Y in tension shown). Yield stresses in X and Y directions are calculated based on the 0.2 pct offset stress on the von Mises curve. Flow stress in the X and Y directions is calculated at the value of effective strain corresponding to a peak in the von Mises curve. Effective strains corresponding to the yield stress and flow stress are shown by the dashed-dotted lines.

directions ($\sigma_x = \sigma_1$, $\sigma_y = \sigma_2$). The z coordinates of the atoms are scaled so as to maintain a constant stress of $\sigma_3 = \sigma_z = 1$ GPa in the Z direction. Figure 6 illustrates the offset and flow stress definitions for unbalanced deformation with compression in X and tension in Y . It can be seen that the stresses in the X and Y directions are initially at 1 GPa and evolve linearly during the deformation prior to yielding. The stress in the Z direction is held constant at 1 GPa. The calculated values of the yield stresses and the flow stresses in the X and Y directions for various loading combinations are plotted in Figures 7(a), and (b), respectively. The yield surface is similar to that calculated at zero pressure, and can be well described using the von Mises-type ellipse. The center of the ellipse is shifted from the ideal value (1,1) by a very small amount α in the third quadrant due to the inherent asymmetry in tension and compression. The yield stress (σ_y) and flow stress (σ_f) values for the fitted ellipse are calculated from the shifted center of the ellipse, as shown in Figures 7(a) and (b), respectively. The lengths of the major and minor axes for the fitted ellipse are tabulated in Table II along with the shift in the center of the ellipse for the yield and flow surfaces. The fitting parameters give the length of the minor axis to be 1.075 GPa, which compares very well with the value of ~ 1.13 GPa predicted by a traditional von Mises ellipse using σ_y . Similarly, the length for the major axis for the yield stress ellipse is calculated to be 2.15 GPa, which is slightly larger than the value of ~ 1.95 GPa predicted by a traditional von Mises ellipse using σ_y . Similarly, the flow stress ellipse has a minor axis of 1.60 GPa, which agrees very well with the value of

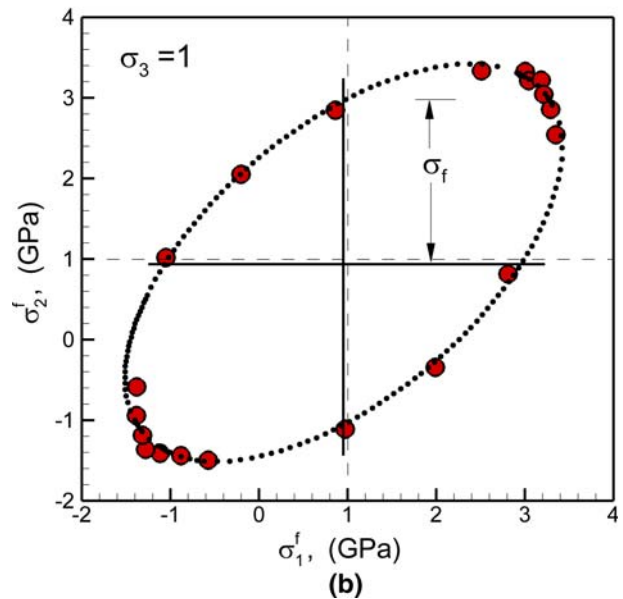
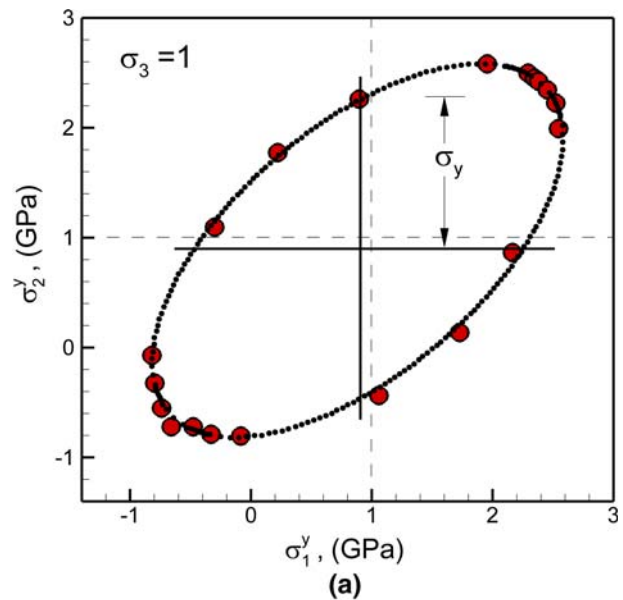


Fig. 7—Plot of the locus of (a) yield stress (0.2 pct offset stress) values and (b) flow stress (peak value of stress) values for biaxial loading in the X and Y directions and constant stress of $\sigma_z = 1$ GPa. Dotted ellipse fitted to the data suggests a von Mises-type yield surface. Solid lines indicate the shifted center of the ellipse to account for the tension-compression strength asymmetry.

~ 1.63 GPa predicted by a traditional von Mises ellipse using σ_f . The length of the major axis for the flow stress ellipse is calculated to be 3.10 GPa, which is slightly larger than the value of ~ 2.83 GPa predicted by a traditional von Mises ellipse using σ_f .

C. Biaxial Yield Surface at $\sigma_z = -1$ GPa

To calculate the yield stresses at a stress of -1 GPa in the Z direction, the system is first equilibrated for 100 ps at a pressure of $P = 1$ GPa. As a result, the stresses in the X , Y , and Z directions are equilibrated at -1 GPa

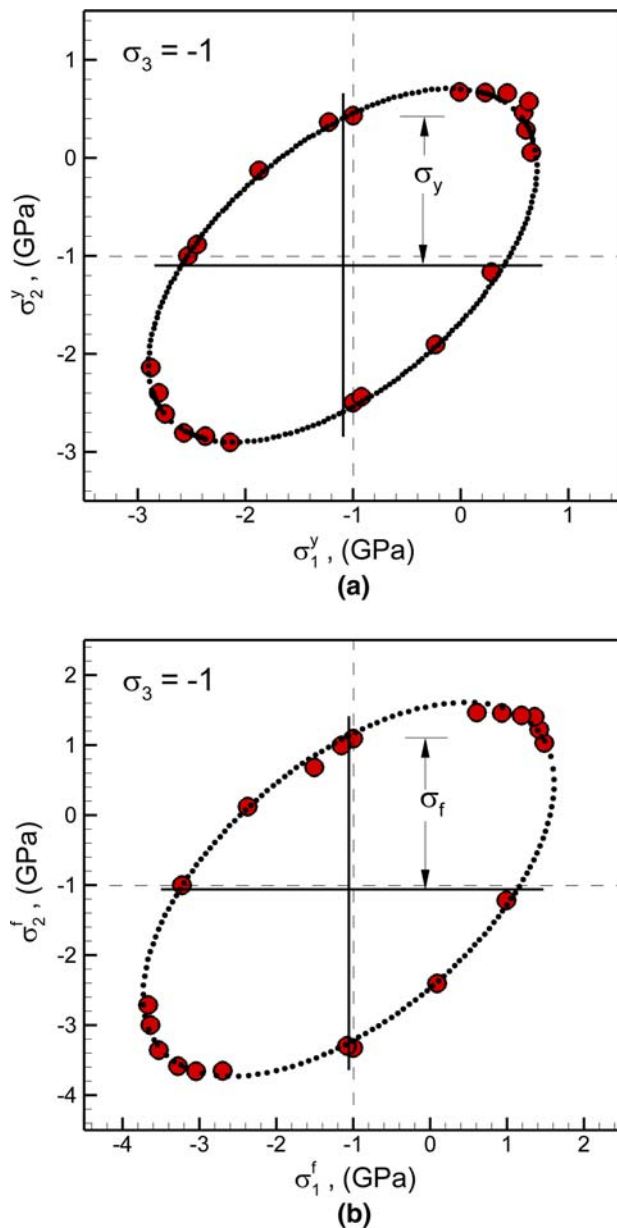


Fig. 8—Plot of the locus of (a) yield stress (0.2 pct offset stress) values and (b) flow stress (peak value of stress) values for biaxial loading in X and Y directions and constant stress of $\sigma_z = -1$ GPa. Dotted ellipse fitted to the data suggests a von Mises-type yield surface. Solid lines indicate the shifted center of the ellipse to account for the tension-compression strength asymmetry.

prior to deformation. Deformation is then carried out as discussed earlier. The locus of the yield and flow stresses in the X and Y directions at $\sigma_z = -1$ GPa is shown in Figures 8(a) and (b), respectively. The calculated values of the yield stresses and flow stresses in the X and Y directions for various loading combinations are plotted in Figures 8(a), and (b), respectively. The yield surface is similar to that calculated at zero pressure, and can be well described using the von Mises-type ellipse. The center of the ellipse is shifted from the ideal value $(-1, -1)$ by a very small amount α in the third quadrant due to the inherent asymmetry in tension and compression.

The lengths of the major and minor axes are tabulated in Table II along with the shift in the center of the ellipse for the yield and flow surfaces. The fitting parameters for the yield stress locus give the length of the minor axis to be 1.2 GPa, which compares very well with the value of ~ 1.22 GPa predicted by a traditional von Mises ellipse using σ_y . The fitting result also gives the length for the major axis to be 2.25 GPa, which is slightly larger than the value of ~ 2.12 GPa predicted by a traditional von Mises ellipse. Similarly, the flow stress ellipse has a minor axis of 1.66 GPa, which agrees very well with the value of ~ 1.70 GPa predicted by a traditional von Mises ellipse using σ_y . The length of the major axis for the flow stress ellipse is calculated to be 3.35 GPa, which is slightly larger than the value of ~ 2.95 GPa predicted by a traditional von Mises ellipse.

D. 3-D Yield Surface

A full 3-D yield surface can be obtained by superpositioning all the yield and flow surfaces on top of each other along the Z axis. The superpositioning in two dimensions for the yield and flow surfaces is shown in Figures 9(a) and (b), respectively. It can be seen that the ellipses are symmetric along the $\sigma_1 = \sigma_2$ axis. This symmetry is inherently predicted by the von Mises yield criterion. The minor axis of the yield stress ellipse, however, appears to be fluctuating. This variation in the minor axis of the calculated ellipses may be attributed to the fluctuation in the yield stress values calculated using the 0.2 pct offset in the stress-strain curves.^[22] The full surface in three dimensions for the yield stresses and flow stresses is shown in Figures 10(a) and (b), respectively. The ellipses together can be seen to form a cylinder that is symmetric around the hydrostatic axis.

The von Mises-type criterion is typically applied to polycrystalline metals in which the deformation mechanism is dominated by dislocation-induced plasticity. Nanocrystalline metals in the inverse Hall–Petch regime show a significant contribution to plastic deformation from GB sliding. The results discussed here suggest the von Mises-type criterion be applicable to predicting yield behavior at ultrafine grain sizes for deformation at ultrahigh strain rates. Deformation at ultrahigh strain rates limits the GB sliding contribution, rendering the dislocations to be the dominant carriers of plasticity. The small deviation in the aspect ratio of the fitted ellipses can be attributed to the small contribution from GB sliding that may still exist.

V. CONCLUSIONS

Large-scale MD simulations are carried out to understand the macroscopic deformation behavior of nanocrystalline Cu with a grain size of 6 nm at high strain rates. Three aspects of deformation behavior are studied: the tension-compression strength asymmetry, the biaxial yield surface, and the 3-D yield surface. The MD simulation results suggest that strength asymmetry is sensitive to the strain rates used. Higher strain rates give a greater asymmetry, with the material being stronger in

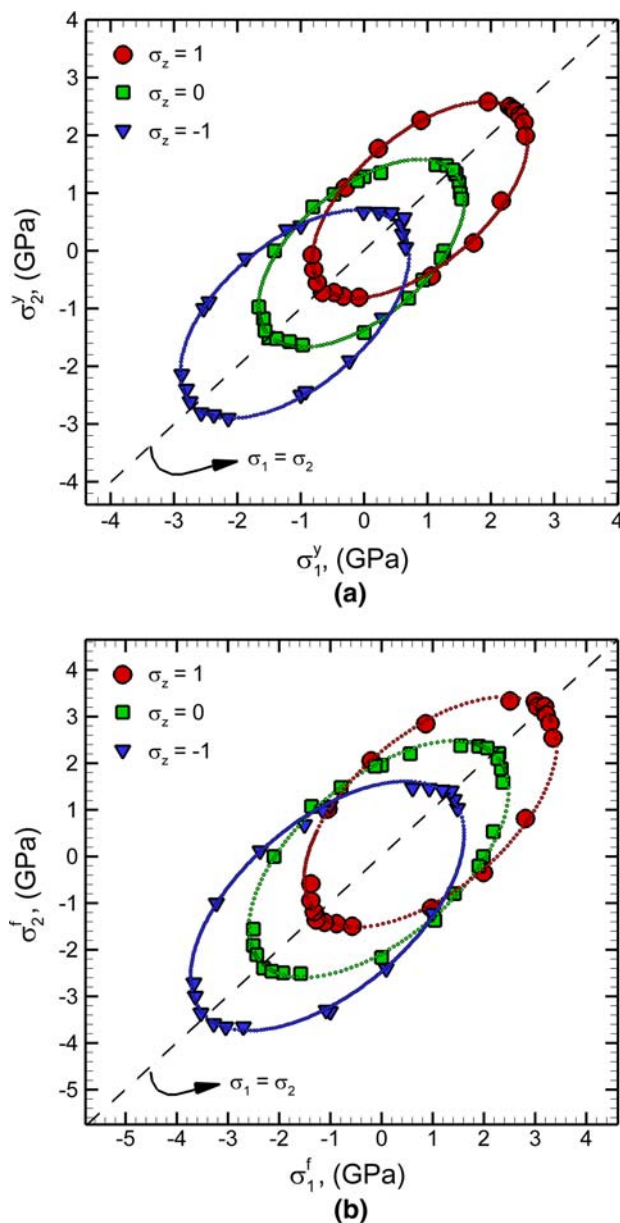


Fig. 9—Superposition of (a) yield stress (0.2 pct offset stress) surface and (b) flow stress (peak value of stress) surface at various values of constant Z stress (σ_z). Ellipses are symmetric along the $\sigma_1 = \sigma_2$ axis, as predicted by the von Mises yield criterion.

tension as compared to tension. The calculated biaxial yield surface for the yield and flow stresses can be fit to an ellipse, suggesting the applicability of a von Mises-type yield criterion. The aspect ratio of the calculated ellipse differs very slightly from that for the ellipse predicted using the traditional von Mises yield criterion. These results indicate that the von Mises-type yield criterion may be used to study deformation at high strain rates for nanocrystalline Cu at grain sizes in the inverse Hall–Petch regime. The applicability of the von Mises yield criterion at ultrahigh strain rates is attributed to the limited GB sliding contribution to plastic deformation at ultrahigh strain rates. Plasticity is therefore controlled by dislocations at high strain rates.

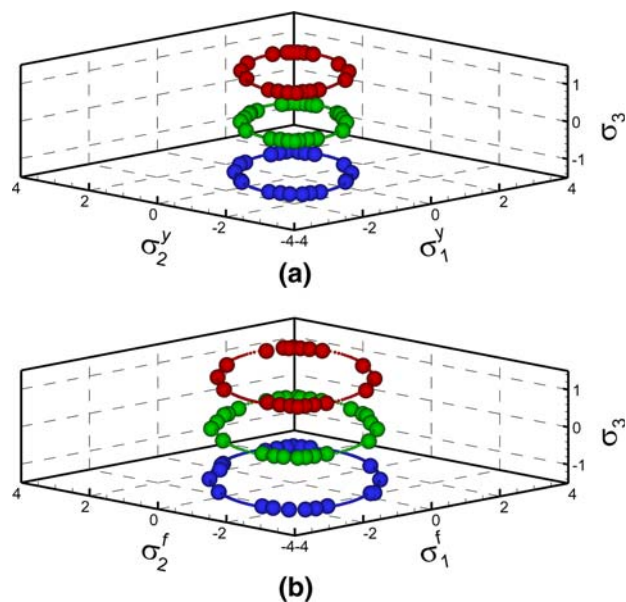


Fig. 10—Plot of 3-D surface: (a) yield stress (0.2 pct offset stress) surface and (b) flow stress (peak value of stress) surface at various values of constant Z stress (σ_z). Ellipses form a cylinder in three dimensions and indicate the validity of the von Mises yield criterion for plastic-yield behavior of nanocrystalline Cu at high strain rates.

The results discussed here do not suggest the von Mises criteria for quasi-static deformation of ultrafine-grain-size nanocrystalline metals. Significant work is needed to evaluate the contributions of GB sliding to plasticity under multiaxial loading conditions and, in turn, the yield criterion to predict the macroscopic behavior of these metals at quasi-static loading conditions.

ACKNOWLEDGMENT

The research is supported by the Army Research Office (ARO) through the National Research Council Research Associateship Program.

REFERENCES

1. K.J. Hemker: *Science*, 2004, vol. 304, pp. 221–23.
2. V. Yamakov, D. Wolf, S.R. Phillpot, A.K. Mukherjee, and H. Gleiter: *Nat. Mater.*, 2002, vol. 1, pp. 45–49.
3. V. Yamakov, D. Wolf, M. Salazar, S.R. Phillpot, and H. Gleiter: *Acta Mater.*, 2001, vol. 49, pp. 2713–22.
4. H. Van Swygenhoven, M. Spaczer, and A. Caro: *Acta Mater.*, 1999, vol. 47, pp. 3117–26.
5. H. Van Swygenhoven and P.M. Derlet: *Phys. Rev. B*, 2001, vol. 64, p. 224105.
6. P.M. Derlet and H. Van Swygenhoven: *Scripta Mater.*, 2002, vol. 47, pp. 719–24.
7. A. Hasnaoui, H. Van Swygenhoven, and P.M. Derlet: *Phys. Rev. B*, 2002, vol. 66, p. 184112.
8. H. Van Swygenhoven, M. Spaczer, A. Caro, and D. Farkas: *Phys. Rev. B*, 1999, vol. 60, pp. 22–25.
9. D.W. Brenner: *Computer Modeling of Nanostructured Materials*, 2nd ed., Carl Koch, ed., Noyes Publications, Norwich, NY, 2006.
10. G.F. Dieter: *Mechanical Metallurgy*, 3rd ed., McGraw Hill, New York, NY, 1986.
11. H. Van Swygenhoven: *Science*, 2002, vol. 296, pp. 66–67.

12. J. Schiotz and K.W. Jacobsen: *Science*, 2003, vol. 301, pp. 1357–59.
13. V. Yamakov, D. Wolf, S.R. Phillpot, A.K. Mukherjee H. Gleiter: *Philos. Mag. Lett.*, 2003, vol. 83, pp. 385–93.
14. K.S. Kumar, H. Van Swygenhoven, and S. Suresh: *Acta Mater.*, 2003, vol. 51, pp. 5743–44.
15. D. Wolf, V. Yamakov, S.R. Phillpot, A. Mukherjee H. Gleiter: *Acta Mater.*, 2005, vol. 53, pp. 1–40.
16. D. Jia, K.T. Ramesh, E. Ma, L. Lu, and K. Lu: *Scripta Mater.*, 2001, vol. 45, pp. 613–20.
17. E.M. Bringa, A. Caro, Y. Wang, M. Victoria, J.M. McNaney, B.A. Remington, R.F. Smith, B.R. Torralva, and H. Van Swygenhoven: *Science*, 2005, vol. 309, pp. 1838–41.
18. R.W. Hertzberg: *Deformation and Fracture Mechanics of Engineering Materials*, 4th ed., Wiley & Sons, New York, NY, 1996.
19. T.H. Courtney: *Mechanical Behavior of Materials*, McGraw-Hill, New York, NY, 1990.
20. N.Q. Vo, R.S. Averbach, P. Bellon, S. Odunuga, and A. Caro: *Phys. Rev. B*, 2008, vol. 77, p. 134108.
21. A.C. Lund, T.G. Nieh, and C.A. Schuh: *Phys. Rev. B*, 2004, vol. 69, p. 012101.
22. A.C. Lund and C.A. Schuh: *Acta Mater.*, 2003, vol. 51, pp. 5399–5411.
23. C.A. Schuh and A.C. Lund: *Nat. Mater.*, 2003, vol. 2, pp. 449–52.
24. A.C. Lund and C.A. Schuh: *Acta Mater.*, 2005, vol. 53, pp. 3193–3205.
25. E. Moshe, S. Eliezer, E. Dekel, A. Ludmirsky, Z. Henis, M. Werdiger, I.B. Goldberg, N. Eliaz, and D. Eliezer: *J. Appl. Phys.*, 1998, vol. 83, pp. 4004–11.
26. G.I. Kanel, S.V. Razorenov, A.V. Utkin, V.E. Fortov, K. Baumung, H.U. Karow, D. Rusch, and V. Licht: *J. Appl. Phys.*, 1993, vol. 74, pp. 7162–65.
27. S. Eliezer, I. Gilath, and T. Bar-Noy: *J. Appl. Phys.*, 1990, vol. 67, pp. 715–24.
28. H. Tamura, T. Kohama, K. Kondo, and M. Yoshida: *J. Appl. Phys.*, 2001, vol. 89, pp. 3520–22.
29. E. Moshe, S. Eliezer, E. Dekel, Z. Henis, A. Ludmirsky, I.B. Goldberg, and D. Eliezer: *J. Appl. Phys.*, 1999, vol. 86, pp. 4242–48.
30. P.M. Derlet and H. Van Swygenhoven: *Phys. Rev. B*, 2003, vol. 67, p. 014202.
31. S. Kumar, S.K. Kurtz, J.R. Banavar, and M.G. Sharma: *J. Stat. Phys.*, 1992, vol. 67, pp. 523–51.
32. C.L. Kelchner, S.J. Plimpton, and J.C. Hamilton: *Phys. Rev. B*, 1998, vol. 58, pp. 11085–88.
33. A.F. Voter: in *Intermetallic Compounds: Principles and Practice*, J.H. Westbrook and R.L. Fleischer, eds., Wiley & Sons, New York, NY, 1994, vol. 1, p. 77.
34. J.A. Zimmerman, H. Gao, and F.F. Abraham: *Modell. Simul. Mater. Sci. Eng.*, 2000, vol. 8, pp. 103–15.

Reproduced with permission of the copyright owner. Further reproduction prohibited without permission.